Development of fundamental technologies for motors in Technology Research Association of Magnetic Materials for High-Efficiency Motors (MagHEM).

Yoshinari Asano, Yoshihito Sanga, Shintarou Araki, Michihiro Nakagawa, Akio Yamagiwa
(Daikin Industries, Ltd.)
Shigeo Morimoto, Masayuki Sanada, Yukinori Inoue
(Osaka Prefecture University)

The Technology Research Association of Magnetic Materials for High-Efficiency Motors (MagHEM) was founded in 2012 to develop the innovative high-performance magnets without/less rare-earth materials which exceed current magnets with rare-earth materials in performance, the high-efficiency soft magnetic materials (Iron core) for internal loss reduction, and compact high-efficiency motors.

Targets of R&D are new magnets exceeding Neodymium magnets with 2 times in (BH)max (180℃), and high efficiency motors with 40% reduction in loss, 40% improvement in power density using new magnets.

This paper investigates the performance of three modified versions of IPMSMs typically used in automotive applications and compares them with a reference model. The modified IPMSMs use a strong magnet model designed to have the properties of NdFe12Nx, which is a novel hard-magnetic compound developed by Hirayama et al. (1). Table I shows the motor specifications, and Fig. 1 shows the cross-sectional analysis model with three types of rotor structures(2)(3). Model B and model C achieved the target of motor in FEA, and model C could meet the strength to centrifugal force.

Acknowledgments
This article is based on results obtained from the Future Pioneering Program "Development of magnetic material technology for high-efficiency motors" commissioned by the New Energy and Industrial Technology Development Organization (NEDO).

Reference

1) Y. Hirayama, Y.K. Takahashi, S. Hirosawa, and K. Hono: “NdFe12Nx Hard-Magnetic Compound with High Magnetization and Anisotropy Field”, MATERIALIA, Vol.95, pp.70–72 (2015)
2) Y. Shimizu, S. Morimoto, M. Sanada, Y. Inoue: “Influence of Permanent Magnet Properties and Arrangement on Performance of IPMSMs for Automotive Applications”, IEEJ Journal of Industry Applications, Vol.6 No.6 pp.1-8(2017)
3) R. Imoto, M. Sanada, S. Morimoto, Y. Inoue: "Study on Mechanical Strength Improvement of Rotor in Compact and High Speed 2-layer IPMSM for HEV Applications", 2018 Kansai Joint Convention of Institutes of Electrical Engineering, G4-17 (2018)

TABLE I MOTOR SPECIFICATIONS

		Reference model	Model A	Model B	Model C
Number of pole/slot		8/48			
Stator diameter (mm)		264		210	
Stack lengsh (mm)		50		54	
Maximus speed (p.u.)		1		1.8	
Rotor Structure		1V	2D		
Iron core	B_{50}(p.u.)	1	0.888		
	$W_{10/50}$(p.u.)	1	0.556		
	Yield stress(p.u.)	1	1.5		
PM material	Remanence (140℃) (T)	1.04	1.39		
	Coercivity (kA/m)	784	1052		
	Wolume (cm^3)	100		69	

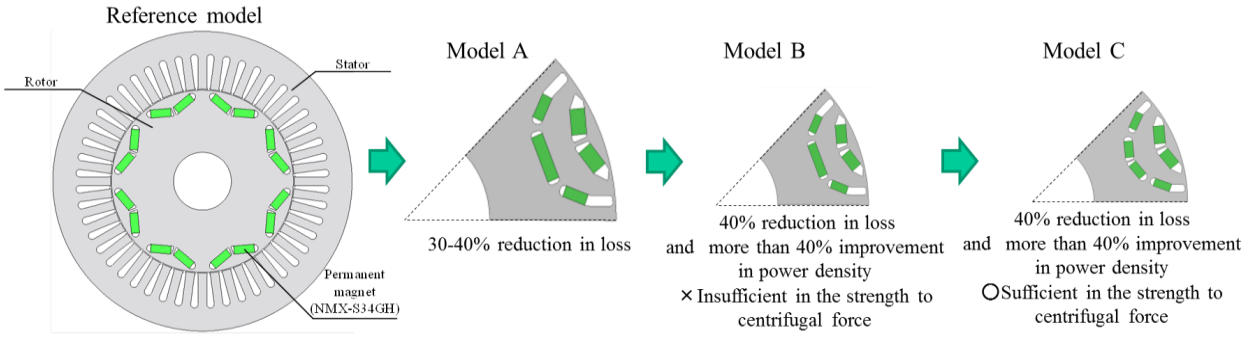

Fig.1. Rotor structure and result of analysis

Development of Nd reduced high coercivity magnet and expectation for future research

Tetsuya Shoji

Toyota Motor Corporation, Advanced Material Engineering Div.
Technology Research Association of Magnetic Materials for High-Efficiency Motors (MagHEM)

1.Background

Recently, vehicle electrification expands rapidly. It is well known that electrified vehicle has additional component compare to conventional gasoline vehicle, i.e. battery, inverter and electric motor. At this moment, supply and demand seems to be acceptable for all additional electric component. However, most of future forecast says that amount of electrified vehicle become two to five times larger than current vehicle sales. This means that we need number of electrified unit, at least, more than two times compare to current demand. For example, IEA scenario described in Energy Technology Perspective 2017 forecasts electrified vehicle increase from 14 million in 2020 to 40 million in 2030 [1]. When we look at even only around vehicle technological shift, it is easy to forecast enormous number of rare-earth magnet will be needed. From this circumstance, we research coerciviy mechanism of rare-earth magnet and consider what we can do for balancing global supply and demand of rare-earth materials. In these ten years, we discovered molten Nd based alloy with low melting point infiltrate spontaneously into bulk magnet and enhance coercivity in 2010[2,3]. Using established technique, we vary coercivity by varying nano-structure of magnet samples for understanding coercivity mechanism. From our research activity, we successfully fabricate relatively high coercivity magnet than expected from rare-earth composition, at that moment we focused on Nd-Ce, in 2013[4,5]. Then we move to investigate intrinsic properties to understand role of rare-earth element for magnetization and curie temperature. All attempts that we made for understanding coercivity mechanism [6,7,8] inspire ideas for development of Nd reduced high coercivity magnet to us.

2.How to realize high coercivity with reduced Nd amount

In order to reduce Nd from NdFeB magnet, we focused on light rare earth (here after LRE) Lanthanum and Cerium. It is well known that adding substituting from Nd to LRE, both magnetization and anisotropy are weakened and performance get worse. Therefore, we noticed mechanism of magnetic properties and combining three techniques, two for nano-structural control and one for alloying technique, for exhibiting high performance even using LRE element [9]. For enhancing coercivity, we control nano-sturcuture of magnet, grain refinement, include magnetic insulation between main phase grains, and Core/Shell structure of grains. When we noticed coercivity model, i.e. Kronmuller's micro-magnetics model, $Hc = \alpha H_a - N_{eff} M_s$. One can easily understand increasing α parameter and/or decreasing N_{eff} work for enhancing coercivity. In this development, we employ grain refinement and magnetic insulation for improving N_{eff}, smaller is better in this case. Furthermore, we put magnetically harder shell, Nd enriched $RE_2Fe_{14}B$ phase, for each grain.to enhance α value. From TEM/EDX observation, one can easily found that Nd enriched region located at surface of each grains and poor in inside grain. This nano-structural control is same as former work reported Ito et al [5]. For improving magnetization, we adopt compositional design for magnet. We start with Nd-Ce alloyed $RE_2Fe_{14}B$ phase, it is well known that magnetization decrease with alloying Ce to $RE_2Fe_{14}B$ phase. In order to slowing deterioration of magnetization by Ce, we focused on La as co-alloying element. Co-alloying La to Nd-Ce seems to have good effect to magnetization relative amount of LRE element of $RE_2Fe_{14}B$ phase.

3. Performance of magnet and discussion

Temperature dependence of coercivity of Nd reduced high coercivity magnet are shown in Fig.1. Comparing NdFeB and Ce alloyed and Ce-La co-alloyed magnet, temperature dependence of coercivity, LRE alloyed magnets, Ce alloyed and Ce-La co-alloyed magnet, are better than NdFeB magnet especially in temperature range around 373K. From Fig.1, Nd infiltrated samples show higher coercivity, therefore it seems that Nd enriched shell harden grain

surface magnetically and enhance coercivity. In Fig.2, Temperature dependences of normalized magnetization of various sample with different composition are shown. Magnetizations are normalized by room temperature value and several Nd reduced composition samples are plotted. When we look at temperature dependence of magnetization, $Ce_2Fe_{14}B$ has worst temperature dependence. When we add La to $Ce_2Fe_{14}B$, temperature dependence, or curie temperature, drastically improved, even though La destabilize $RE_2Fe_{14}B$ phase. This behavior is same as Nd alloying to $Ce_2Fe_{14}B$. Finally, we co-alloy Ce and La to $Nd_2Fe_{14}B$, temperature dependence of magnetization seems to have peak in certain ratio of Ce and La, or La improve magnetization in elevated temperature. From our experimental results, temperature dependence of both coercivity and magnetization seems to be affected by LRE alloying.

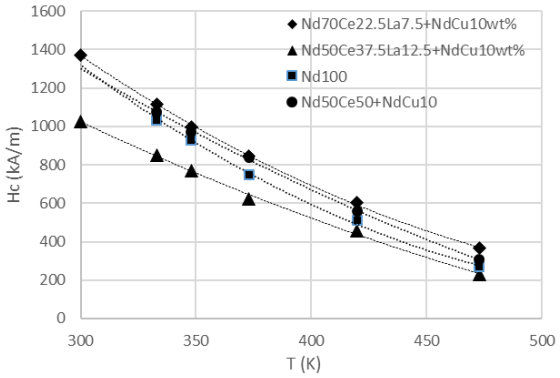

Fig.1 Temperature dependence of various magnet coercivity. Sample name correspond to RE composition. Sample with NdCu infiltration. Infiltration condition is 853K 165min.

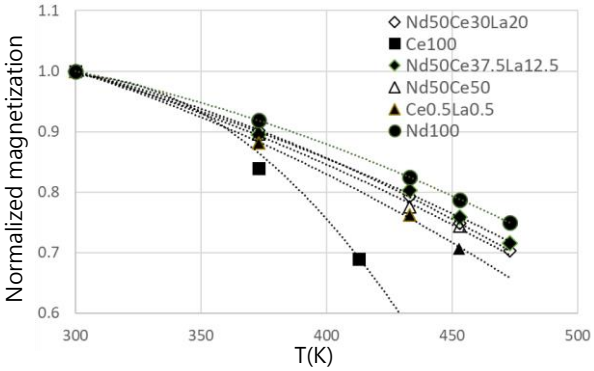

Fig.2 Temperature dependence of normalized magnetization. Sample name correspond to RE composition

Acknowledgement

This work was partly supported by the future pioneering program Development of Magnetic Material Technology for High-efficiency Motors commissioned by the New Energy and Industrial Technology Development Organization (NEDO).

Reference

1) Energy Technology Perspective 2017; IEA
2) Patent: JP 5196080
3) H. Sepehri-Amin et al; Acta Materialia 61 (2013), pp. 6622-6634
4) Patent: JP 6183457
5) M. Ito et al; AIP Advances **6**, 056029 (2016);
6) S. Bance et al; Journal of Applied Physics **116**, 233903 (2014);
7) S. Bance et al; Appl. Phys. Lett. **104**, 182408 (2014);
8) S. Bance et al; Hard magnet coercivity, Proceedings of the 23rd International Workshop on Rare earth and Future Permanent Magnets and Their Appications (REPM2014),
9) Toyota Global News Room, Feb. 20th, 2018, URL: https://global.toyota/en/newsroom/corporate/21139684.html

Powder neutron diffraction study for magnetism of rare-earth in $(Nd,Ce,La)_2Fe_{14}B$

Takafumi Hawai[1], Masao Yano[2], Tetsuya Shoji[2], James Hester[3], Kanta Ono[1]
([1]KEK, [2]Toyota Motor Corp, [3]ANSTO)

Introduction

To reduce expensive Neodymium in rare-earth magnets $Nd_2Fe_{14}B$ without decrease of magnetic properties, cheap Cerium is paid attention. In general, the Ce atom is in non-magnetic Ce^{4+} state. However, when the magnetic Ce^{3+} state is stable, the Ce should work as a substitution for Nd. Previous research reported that the larger ionic radii rare-earth prefer the larger cell volume [1]. The magnetic Ce^{3+} state has larger atomic radii (1.15 Å) than that of Ce^{4+} state (1.01 Å) [2]. Therefore, the La (1.17 Å) is doped as a spacer to stabilize the Ce^{3+} state. Previous powder neutron diffraction study reported that Ce atom in $(La,Ce)_2Fe_{14}B$ has no moment [3]. Following the previous results, in this study, powder neutron diffraction experiments were performed on $(Nd,Ce,La)_2Fe_{14}B$ to evaluate the rare-earth moment and the Ce state.

Experimental

The powder samples of $Nd_2Fe_{14}B$, $(Nd_{0.75}Ce_{0.225}La_{0.075})_2Fe_{14}B$, $(Nd_{0.5}Ce_{0.375}La_{0.125})_2Fe_{14}B$, and $Ce_2Fe_{14}B$ were measured. The mass of samples is 5g each. Diffraction patterns were gathered on the Echidna – High-Resolution Powder Diffractometer in Australia's Nuclear Science and Technology Organization (ANSTO). Natural boron was substituted with ^{11}B due to strong neutron absorption. The wavelength of the neutron is 2.44 Å.

Results

Figure 1 shows an observed diffraction pattern of $(Nd_{0.5}Ce_{0.375}La_{0.125})_2Fe_{14}B$ together with a result of Rietveld analysis. The experimental data was well explained by the calculated pattern. Figure 2 shows the obtained Nd content dependences of rare-earth moments. The moment sizes change linearly at Nd 70 % compounds. In contrast, at Nd 50 %, the moment size of 4*g* site deviates from linear change and increases. The reported rare-earth moments in $(Nd,Ce)_2Fe_{14}B$, shown as open triangles in Fig. 2, quickly decreases with decreasing Nd content [3]. This result suggests that some Ce atoms in 4*g* site are magnetic Ce^{3+} state instead of non-magnetic Ce^{4+} state thanks to the La atom spacer. The details will be discussed.

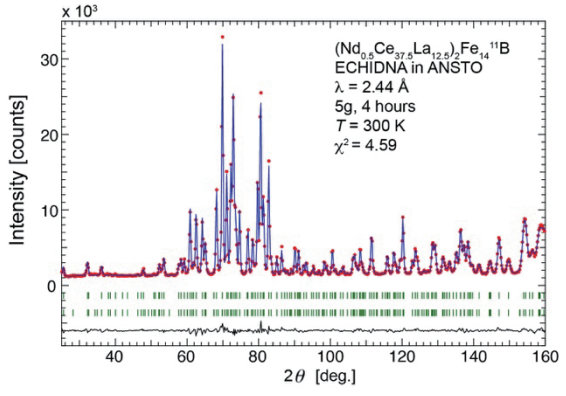

Fig. 1: The diffraction pattern of $(Nd_{0.5}Ce_{0.375}La_{0.125})_2Fe_{14}B$ together with Rietveld refinement results at 300 K.

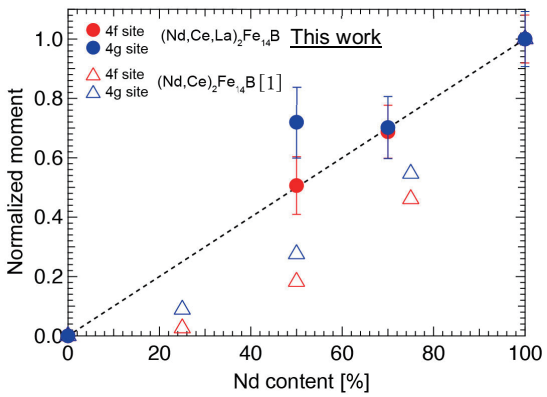

Fig. 2: The Nd content dependence of rare-earth moments at 4*f* and 4*g* site. The Moments shows here are normalized by the Nd moments of $Nd_2Fe_{14}B$.

Reference

1) K. Saito, *et al*., J. Alloy. Compd. **721, 476** (2017).
2) R. D. Shannon, Acta Crystallographica **A32**, 751 (1976).
3) C. V. Colin *et al*., APL **108**, 242415 (2016)

High-resolution synchrotron X-ray powder diffraction study of lattice constants of $Nd_2Fe_{14}B$ phase in Nd-Fe-B sintered magnets

S. Kobayashi[1,2], A. Martin-Cid[1,2], K. Toyoki[1,2], H. Okazaki[1,2], S. Hirosawa[2] and T. Nakamura[1,2]
[1]Japan Synchrotron Radiation Research Institute, 1-1-1 Kouto, Sayo, 679-5198, Japan.
[2]Elements Strategy Initiative Center for Magnetic Materials, National Institute for Materials Science, Tsukuba 305-0047, Japan.

[Purpose]

The high-performance Nd-Fe-B magnets have been receiving considerable attention due to their outstanding magnetic properties. Owing to large magnetic moments of Fe atoms, the main phase of $Nd_2Fe_{14}B$ exhibits large spontaneous volume magnetostriction of about 2%. In addition, the spontaneous magnetostriction is highly anisotropic as shown in Fig. 1. Andreev *et al*. have reported that the linear spontaneous magnetostrain along the *a*-axis (λ_a) is about 4.5 times larger than that along the *c*-axis (λ_c).[1)] However, Yang *et al*. have reported that λ_a is only 1.7 times larger.[2)] It is very curious to find out the clear reason for this discrepancy, since magnetostriction should be intrinsic properties related to magnetization and magnetoelastic-coupling coefficients. In our previous study, [3)] we showed the temperature dependences of the lattice constants for each constituent phase in a Nd-Fe-B-Cu anisotropic as-sintered magnet and found that they change differently from those expected for the pristine metal or compounds. This result indicates that lattice constants are influenced by some additional factors. In order to acquire a better understanding about the changes in the lattice constants, we have conducted high-resolution synchrotron XRD measurements in several kinds of samples.

[Experimental]

Isotropic and anisotropic Nd-Fe-B-Cu as-sintered magnets, their powdered samples, and powdered single crystals were used in this study. The preparation methods have been already reported.[3,4)] The synchrotron XRD measurements of as-sintered magnets were conducted using rectangular rod-shaped samples (0.2 × 0.2 × 5 mm^3). Synchrotron XRD profiles were collected at the BL02B2 beamline at SPring-8.

[Results]

Above T_C, the lattice constants of the $Nd_2Fe_{14}B$ phase in as-sintered magnets, their powdered samples, and powdered single crystals showed a similar temperature variation. Lattice constants of all the samples exhibited a clear anomaly around the same temperature of $T_C \simeq 580$ K and exhibited an invar-like expansion below T_C, which is similar to previous reports [see Fig. 1].[1,2)] Interestingly, the behaviour of the lattice constants below T_C was different, and the *a*-axis increased and *c*-axis decreased in the following order: the isotropic as-sintered magnet, anisotropic as-sintered magnet, their powdered samples, and powdered single crystals. In addition, a broadening of the diffraction peaks was observed for isotropic and anisotropic as-sintered magnets below T_C, while this broadening was negligibly small for powdered samples. The Williamson-Hall analysis clarified that the origin of the peak broadening was likely due to internal lattice strain in the sintered magnets. These results indicate that there exists an anisotropic stress applied to the $Nd_2Fe_{14}B$ crystal grains in the sintered magnets. Our experimental results settled the problem of discrepancy in λ_a/λ_c.

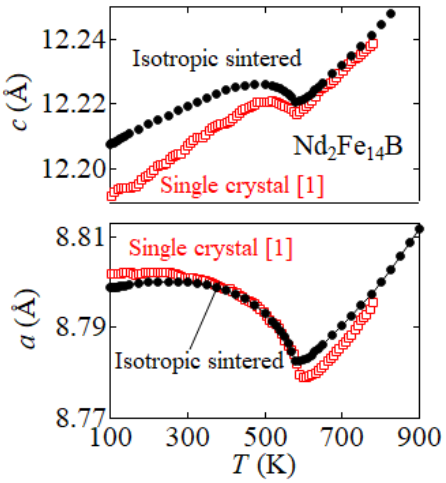

Fig.1 Temperature variation of lattice constants of $Nd_2Fe_{14}B$ in isotropic Nd-Fe-B-Cu as-sintered magnets in comparison with previous reports.[1)]

We thank T. Nishiuchi of Hitachi Metals, Ltd. for supplying the samples. A part of this work is supported by ESICMM under the outsourcing project of MEXT.

References

1) A.V. Andreev *et al*., Sov. Phys. Solid State. **27,** 987 (1985). 2) N. Yang *et al*., J. Magn. Magn. Mater. **295**, 65 (2005).
3) N. Tsuji *et al*., Acta Mater. **154**, 25 (2018). 4) S. Hirosawa *et al*., J. Appl. Phys. **59**, 873 (1986).

Microstructure and coercivity of grain boundary diffusion processed Dy-free and Dy-containing Nd-Fe-B sintered magnets

T.-H Kim[1], T. T. Sasaki[1], T. Ohkubo[1], Y. Takada[2], A. Kato[3], Y. Kaneko[2], and K. Hono[1]
[1]Elements Strategy Initiative Center for Magnetic Materials, National Institute for Materials Science, Tsukuba-city, Ibaraki 305-0047, Japan
[2]Toyota Central R&D Labs., Inc., 41-1, Nagakute 480-1192, Japan
[3]Toyota Motor Corp., Advanced Material Engineering Div., Susono 410-1193, Japan

Achieving a high coercivity, $\mu_0 H_c$, above 3.0 T at room temperature is important for Nd-Fe-B permanent magnets for the application to traction motors of electric vehicles and wind turbines to avoid thermal demagnetization. Grain boundary diffusion (GBD) is promising to achieve the high coercivity without the significant loss of remanence that cannot be avoided with Dy alloying. In the GBD process, heavy rare-earth element (HRE) is diffused from the surface of the bulk along the grain boundaries, thereby forming HRE-rich shell on the surface of the $Nd_2Fe_{14}B$ main phase. This contributes to the coercivity increment. However, the coercivity cannot reach 3.0 T by the GBD process alone unless the initial sintered magnets are alloyed with Dy; a substantial amount of Dy must be alloyed in the base magnets in order to achieve the high coercivity of 3.0 T after the GBD process[1]. In the present study, we investigated the magnetic and microstructural characteristics of the GBD processed Dy-free and Dy-containing sintered magnets in order to understand the origin of the high coercivity of 3.0 T.

A GBD process was applied to two different sintered magnets with the chemical composition of $Nd_{14.3}Fe_{78.15}B_{6.0}Cu_{0.1}Al_{0.4}Co_{1.0}Ga_{0.05}$ and $Nd_{11.2}Dy_{3.1}Fe_{78.15}B_{6.0}Cu_{0.1}$ $Al_{0.4}Co_{1.0}Ga_{0.05}$ (at.%). The Dy-free and Dy-containing samples have the coercivity of 0.64 and 2.29 T before the GBD process. They were kept in Dy-vapor at 950 °C for 4 h for the GBD treatment followed by the post-diffusion annealing at 520 °C for 1 h. The Dy distributions in these magnets have been investigated via the use of SEM (Carl Zeiss Cross beam 1540EsB) and TEM (FEI Titan G2 80-200).

The coercivity increment, $\Delta\mu_0 H_c$, by the GBD treatment for the Dy-containing magnet was only 0.08 T, which was much smaller than that for the Dy-free magnet of 0.87 T due to the discontinuity of the Nd-rich GB phase in the Dy-containing magnet (Fig. 1). After the subsequent post-diffusion annealing, a substantial coercivity increase was observed, and the $\mu_0 H_c$ of the Dy-containing magnet reached 3.05 T while that of the Dy-free magnet saturates at 2.29 T. One reason for the 3T coercivity in the Dy-containing sample is the formation of the thick GB phase with high Nd content.

Interestingly, we found the formation of a “secondary Dy-rich shell” within the well-known primary Dy-rich shell[2]. The Dy element enriched in the Nd-rich GB phase during the GBD treatment is diffused into the main phase to form the secondary Dy-rich shell during the post-diffusion annealing. Such a secondary Dy-rich shell gave additional rise in the coercivity to 3T due to the increase in the Dy content at the GB phase/$(Nd,Dy)_2Fe_{14}B$ interface.

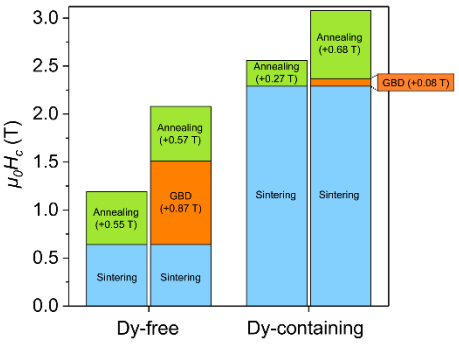

Fig. 1: $\Delta\mu_0 H_c$ of Dy-free and Dy-containing magnets with GBD process steps. For comparison, $\Delta\mu_0 H_c$ of magnets annealed without undergoing the GBD treatment are also displayed.

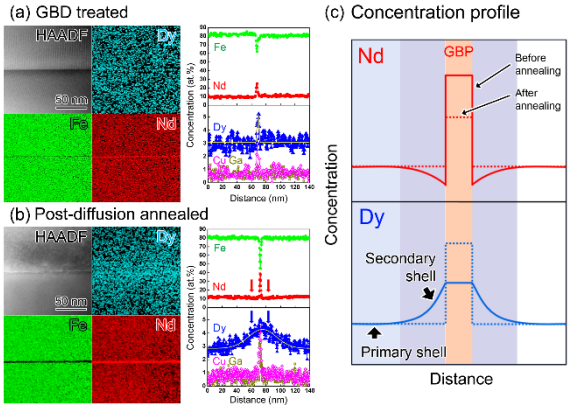

Figure 6: HAADF-STEM image and corresponding EDS elemental maps, and EDS line profiles across GB phase in (a) GBD treated and (b) post-diffusion annealed Dy-free magnet. (c) schematically shows the change in Nd and Dy concentration before and after the post diffusion annealing.

Reference
1) S.-E. Park et al., IEEE Trans. Magn, 47 (2011) 3259-3262
2) T.-H. Kim et al., Acta Mater. 175 (2019) 139-149

Improved coercivity and squareness in bulk hot-deformed magnets by two-step grain boundary diffusion process

Xin Tang,[1] J. Li,[1] H. Sepehri-Amin,[1] T. Ohkubo,[1] K. Hioki,[2] A. Hattori[2] and K. Hono[1]
[1]Elements Strategy Initiative Center for Magnetic Materials, National Institute for Materials Science, Tsukuba 305-0047, Japan
[2]Daido Corporate Research & Development Center, Daido Steel Co., Ltd.

In order to use Nd-Fe-B based permanent magnets for the traction motor of hybrid (electric) vehicles, a coercivity of 0.8 T is required at 160 °C to avoid their thermal demagnetization during operation. To meet this requirement, grain boundary diffusion of RE-based eutectic alloys is employed to improve the coercivity in the hot-deformed magnets. [1)] Recently, Li *et al.* reported a coercivity of ~2.57 T with remanence of 1.38 T in a 2-mm-thick hot-deformed magnet by the grain boundary diffusion of Tb-Nd-Cu alloy. [2)] However, such high performance was demonstrated only using a small piece of samples with a thickness of ~2 mm and a question is whether or not we can apply the process to large bulk samples. Previous reports on conventional Dy-vapor diffusion process in micron-grain sized Nd-Fe-B sintered magnets has shown that the limited diffusion depth results in a poor squareness of demagnetization curves. [3)] In this work, we investigated the method to improve the squareness of demagnetization curves of Nd-HRE-Cu eutectic-diffusion processed 5.6-mm-thick hot-deformed magnets.

The hot-deformed Nd-Fe-B-based magnets with composition of $Fe_{67.1}Pr_{6.7}Nd_{21.2}Co_{3.5}Ga_{0.5}B_1$ (wt.%) were used as starting materials. The samples of × 7 × 5.6 (c-axis) mm^3 in size were covered by the 12 wt.% $Tb_{20}Dy_{10}Nd_{40}Cu_{30}$ ribbons (with respect to mass of hot-deformed magnet) followed by annealing at 750°C for 1.5 h and post-annealing at 650°C for 9h, which is called as “one-step diffusion process”. In comparison, the two-step diffusion process was carried out as follows: the initial samples were covered by the 10 wt.% $Tb_{20}Dy_{10}Nd_{40}Cu_{30}$ ribbons (with respect to the mass of hot-deformed magnet) followed by annealing at 750°C for 1.5 h. Thereafter, the surface of the magnet was polished and the magnet was again covered by 6 wt.% of $Nd_{80}Cu_{20}$ alloy ribbons followed by heat-treatment at 650°C for 9 h. The magnetic properties were studied by pulse BH-tracer.

Fig. 1 shows the demagnetization curves of the one-step and the two-step diffusion processed samples. The coercivity is improved from ~1.14 T in the as-deformed sample to ~2.38 T while remanence degrades from ~1.49 T to ~1.28 T after one-step diffusion procession. In contrast, the coercivity is enhanced to 2.43 T with remanent magnetization reduction to ~1.29 T by the two-step diffusion process. The squareness factor of demagnetization curve is defined as $\mu_0 H_k/\mu_0 H_c$, where $\mu_0 H_k$ is the absolute value of external field when the magnetization equals to 90% of remanent magnetization ($\mu_0 M_r$) and $\mu_0 H_c$ is the coercivity of the sample. The squareness factor was calculated to be ~0.83 for the one-step diffusion processed sample, which is improved to ~0.91 after the two-step diffusion. The origin of the obtained magnetic properties will be discussed based on detailed microstructure characterization.

Reference

1) H. Sepehri-Amin, *et al.*, Acta Mater. 61 (2013) 6622-6634.
2) J. Li, *et al.*, Acta Mater. 161 (2018) 171-181.
3) K. Löewe, *et al.*, Acta Materialia 83 (2015) 248-25.

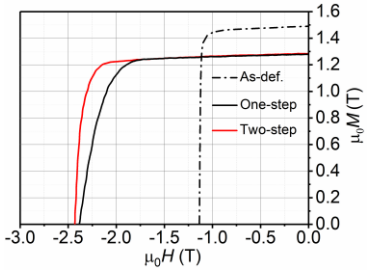

Fig. 1 Demagnetization curves of hot-deformed magnets and diffusion-processed magnets

Theoretical study on the magnetization reversal of rare-earth magnets at finite temperature

A. Sakuma[1],Y. Toga[2,3],T. Miyake[3,4], and S. Miyashita[3,5,6]
([1]Tohoku University, [2]NIMS, [3]ESICMM, [4]AIST, [5]The University of Tokyo, [6]JPS)

In viewpoints from both the energy-efficiency and environment problems, the development of high-performance Nd-Fe-B permanent magnets is strongly desired especially for electric vehicles. It has so far been recognized that one of the important issues to be overcome is suppressing the thermal degradation of their coercivity, H_{C}. As a measure, Dy is currently substituted for part of Nd in Nd-Fe-B sintered magnets. However, this is unfavorable because Dy is expensive and the magnetization decreases owing to the antiparallel coupling between Dy and Fe moments. For these reasons, the microscopic foundations for the magnetization reversal mechanism of Nd-Fe-B magnets are sincerely needed and many theoretical works have been done intensively based on several different approaches.

A direct way to study the hysteresis loop is to employ the Langevin equation so-called stochastic LLG equation which takes into account the thermal fluctuation.[1)] However, the method consumes much computation time to reach the observation time of a few seconds. Alternatively, to handle such a slow relaxation process, usage of the free energy landscape is useful and appropriate. Actually, the magnetization reversal can be interpreted as the transition from metastable magnetic state to a stable state by overcoming the free energy barriers under a reverse magnetic field. The reverse nucleus is formed in this process. To deal with such processes at finite temperature, one needs to evaluate the free energy landscape instead of searching the energy minimum path.[2)]

Recently, we[3)] have succeeded, for the first time, to calculate the free energy $F(T, H_z, M_z)$ of a finite-size particle of $Nd_2Fe_{14}B$ as functions of temperature (T), external magnetic field ($H_z < 0$) and the z-component of the total magnetic moment (M_z) with using replica-exchange Wang-Landau method.[4)] This method enables us to evaluate the $F(T, H_z, M_z)$ with using only the magnetic parameters at zero temperature such as the local magnetic moments (M_i), exchange interactions (J_{ij}) between them and the anisotropy constants (crystal field parameters) all of which can be determined by the first principles calculation.[5)]

Figure 1(a) shows the spatial distribution of the reversed magnetization around the barrier as shown by the arrows in Fig. 1(c). In Fig. 1(b), we show the averaged magnetization density. From these data one can find that the reverse begins at the corner because of the weak exchange field, and then the domain wall propagates toward the center of the particle. Once the $F(T, H_z, M_z)$ is obtained as in Fig. 1 (c), we can calculate, without using any empirical parameter, the energy barrier $F_{\mathrm{B}}(T, H_z)$, activation volume $V_{\mathrm{a}}(T, H_z)$ and viscosity coefficient (fluctuation field) $S_{\mathrm{v}}(T, H_z)$. Taking account of the thermal fluctuation, the coercivity H_{C} in the observation time of one second can be determined from the relation $F_{\mathrm{B}}(T, H_{\mathrm{C}}) = 25.3 k_{\mathrm{B}} T$. Further, we have demonstrated both analytically and numerically that $V_{\mathrm{a}}(T, H_z)$ which is defined as a volume swept out between minimum and maximum energy positions of the domain wall[6)] (corresponding to ΔM_z in Fig. 1(c)) is always given by $-(\partial F_{\mathrm{B}}/\partial H_z)/M_{\mathrm{S}}$, regardless of the form (magnetization reversal model) of $F_{\mathrm{B}}(T, H_z)$. From the data, we found that the $V_{\mathrm{a}}(T, H_z)$ drops sharply with increasing H_z in a low H_z region and goes to a certain constant value as H_z approaches to H_{C}. This implies that $F_{\mathrm{B}}(T, H_z)$ is approximately proportional to $(1 - H_z/H_0)^n$ with n close to unity when $H_z \simeq H_{\mathrm{C}}$, while, for H_z much smaller than H_{C}, n is larger than 2. The result $F_{\mathrm{B}} \propto (1 - H_z/H_0)^n$ ($n \simeq 1$) for Nd-Fe-B magnets seems agreeable with the experimental findings by Givord et al.[7)] and Okamoto et

al.[8] The physical interpretation for $n \simeq 1$ (V_a is nearly independent of H_z) will be given in the conference.

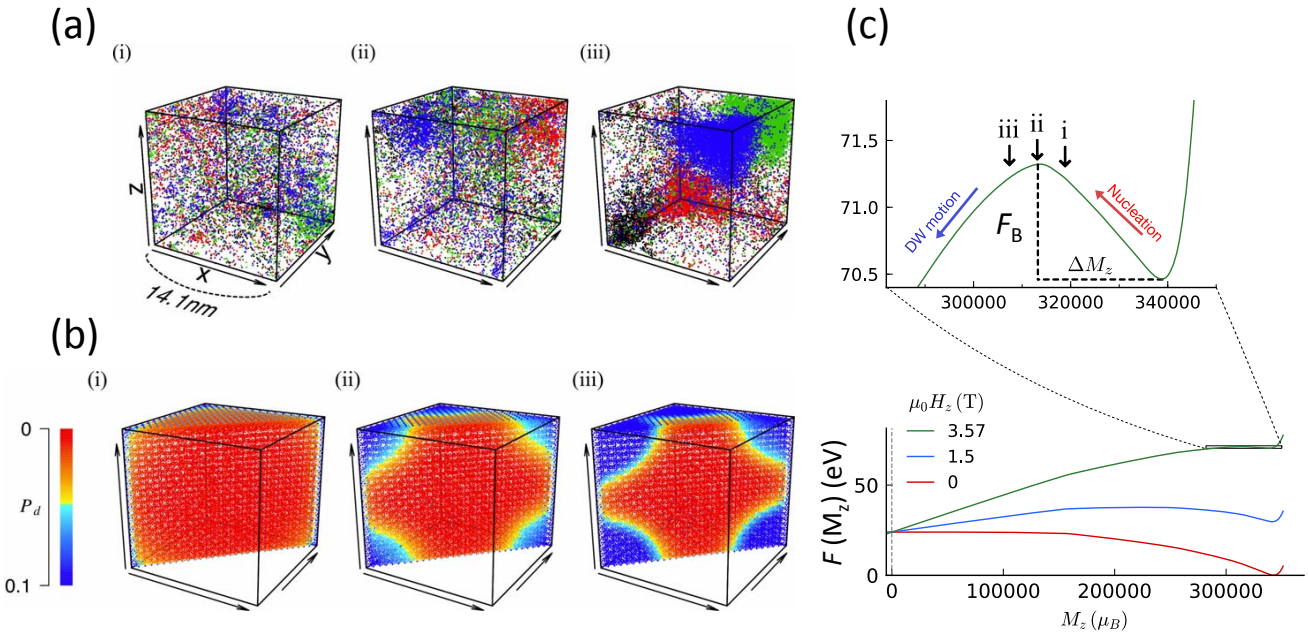

Fig. 1 Free energy landscape simulation of surface nucleation.(a) Snapshots of distributions at the three magnetization points i - iii in the free energy landscape (Fig. 1(c)) simulated by the replica exchange Wang-Landau method for the $Nd_2Fe_{14}B$ isolated particle spin system, whose size is 14.1nm ×14.1nm ×14.6nm (212,536 spins). The dots of each color denote reversed Fe spins in each snapshot. (b) The distributions sliced by (110) plane of the possibility of spin reversal P_d at Fe sites. (c) Free energies as a function of the z-component of the total magnetic moment M_z at $0.46T_C^{cal}$. The blue and green lines are the results of applying reverse magnetic fields H_z along $-z$ direction to the red line.

References

1) M. Nishino et al., Phys. Rev. B **94** (2017) 094429.
2) R. Dittrich et al., J. Magn. Magn. Mater. **250** (2002) 12.
3) Y. Toga et al, in preparation for submission.
4) T. Nogawa et al., Phys. Rev. E **84** (2011) 061107.
5) Y. Toga et al., Phys. Rev. B **94** (2016) 174433.
6) P. Gaunt, J. Appl. Phys. **59** (1986) 4129.
7) D. Givord et al., J. Magn. Magn. Mater. **67** (1987) L281.
8) S. Okamoto et al., J. Appl. Phys. **118** (2015) 223903.

Recent progress in studies on crystalline phases and magnetic domain structures in high coercivity permanent magnets using synchrotron X-rays

T. Nakamura*

(JASRI, *ESICMM)

In the last three decades, synchrotron X-rays have been widely used in materials science. To date, they have become essential means of getting information about crystal structures and electronic and magnetic properties of materials. In the earlier studies, the structural, physical and chemical properties had been investigated mostly in pristine substance like the single crystals or the single phase compounds, whilst the recent applications of the synchrotron X-rays extend to practical materials which are generally polycrystalline and inhomogeneous. In addition, the *in situ* measurements are becoming more popular in order to get better understanding about what happens in materials during manufacturing processes or practical uses.

A study of permanent magnets using the synchrotron X-rays is such a recent subject since magnets are usually inhomogeneous with the microstructure. A Nd-Fe-B sintered magnet has been the strongest permanent magnet since its invention by Sagawa et al. in 1983 [1] and is widely used in many applications such as electric vehicles, wind power generators and voice coil motors, which are crucial for realizing a sustainable society. However, the coercivity mechanism in the Nd-Fe-B sintered magnets remains a debated issue in which the practical coercivity of approximately 1–2 T is rather moderate compared to the value expected from its magnetic anisotropy field of approximately 7.5 T. We have, therefore, carried out the synchrotron based characterizations for the analysis of structural and magnetic properties of the Nd-Fe-B sintered magnets by applying X-ray diffraction (XRD) and X-ray magnetic circular dichroism (XMCD) experiments, respectively. In this talk, I will present recent studies on structural and magnetic properties in high performance permanent magnets using the synchrotron X-rays at SPring-8. I will also illustrate the developments of measurement techniques which have were motivated by the necessity of the characterization of the permanent magnets.

Figure 1 shows the summary of the measurement techniques and their measured examples which have been obtained in studies of the Nd-Fe-B sintered magnets at SPring-8. In the experiment using soft XMCD, the fractured surface in Nd-Fe-B-Cu sintered magnet was investigated to evaluate the magnetic property of the grain boundary (GB) phases directly [2]. This work has clarified that the GB phase which is exposed in the fractured surface shows ferromagnetic at room temperature and have the lower Curie temperature than that of $Nd_2Fe_{14}B$ crystal by about 50 °C. Since this result was recorded using an unfocused soft X-ray beam with the irradiated area of about sub-mm^2 in the sample surface, the magnetic property were detected as the laterally averaged from a number of grains. In order to increase the spatial resolution in the soft XMCD measurement, we have developed a scanning soft XMCD microspectroscopy measurement technique with the apparatus equipped with an 8 T superconducting magnet at BL25SU of SPring-8 [3]. This observation technique using the focused soft X-ray beam with the beam size of about 100 nm makes us possible to visualize magnetic domains with the elemental distribution not only for the flat surface like the polished one but also for the irregular surface like the fractured one. The substantial difference in the magnetic domain reversal is observed for the polished and fracture surfaces [4]. The magnetic domain reversal behavior is also compared with the result of the FORK measurement, showing that the magnetic domain observation is valuable to give an interpretation of the FORK diagram [5]. Regarding the uses of the hard X-rays, we performed the scanning hard XMCD microspectroscopy experiment using the focused X-ray beam as small as 100 nm^2 at BL39XU of SPring-8 [6]. In the magnetic domain observation using the hard X-rays, the surface insensitive observation becomes possible though the deeper probing depth decrease the lateral spatial resolution. More recently, the observation technique for visualizing magnetic domains three dimensionally has been developed using the focused hard X-ray beam. This development directs the future uses of the magnetic domain observation techniques, where the soft and hard X-rays will probe the surface two dimensionally and the interior three dimensionally, respectively. In the structural analysis, the *in situ* XRD

measurement at elevated temperature and the Rietveld analysis have also been applied to studies of the Nd-Fe-B-Cu sintered magnet in order to evaluate the variation of the constituent phases during the annealing process. As the result of the Rietveld analysis, it is implied that dhcp Nd phase in the Nd-Fe-B-Cu sintered magnet contains a certain amount of oxygen and shows the phase transition to the fcc structure when the internal stress is removed [7]. Here, I would like to emphasize that the structure and/or magnetic property of crystalline phases in materials with the microstructure are possibly different from their pristine materials, meaning that the new functional material would be found even in materials which is practically used at present. The synchrotron X-ray measurement technique with the nano-scale resolution will possibly becomes a tool to discover a new material which will make an innovation.

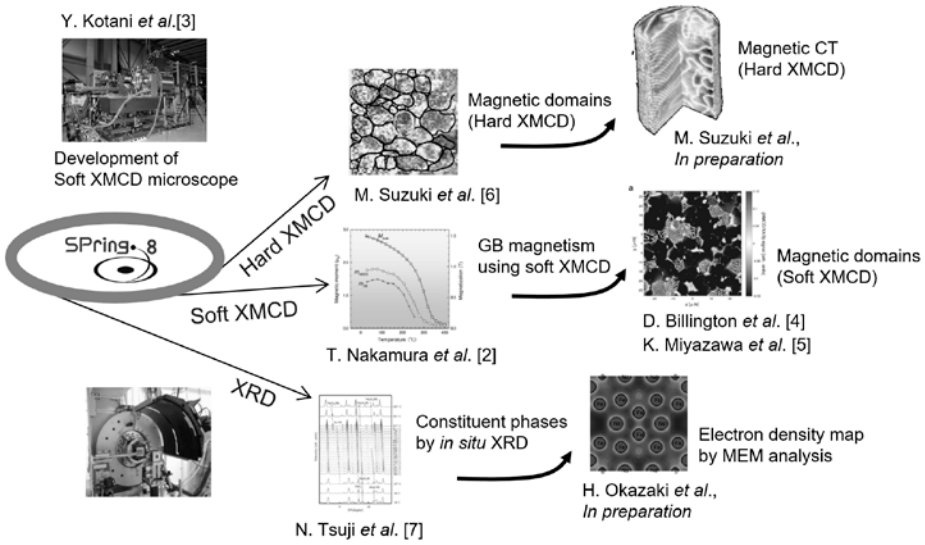

Fig.1 Measured examples in synchrotron X-ray experiments and developed measurements techniques at SPring-8 for studies of permanent magnets.

Acknowledgements

The authors are grateful to Dr. Nishiuchi of Hitachi Metal Ltd. and H. Nakamura of Shin-Etsu Chemical Co., Ltd. for providing the Nd-Fe-B sintered magnet samples for the synchrotron experiments. Part of this work is supported by the Elements Strategy Initiative Center for Magnetic Materials under the outsourcing project of MEXT, and the Japan Science and Technology (JST) Agency, Collaborative Research Based on Industrial Demand (JPMJSK1617).

References

[1] M. Sagawa, S. Fujimura, N. Togawa, H. Hashimoto, and Y. Matsuura, J. Appl. Phys. **55**, 2083 (1984).

[2] T. Nakamura, A. Yasui, Y. Kotani, T. Fukagawa, T. Nishiuchi, H. Iwai, T. Akiya, T. Ohkubo, Y. Gohda, K. Hono, and S. Hirosawa, Appl. Phys. Lett. **105**, 202404 (2014).

[3] Y. Kotani, Y. Senba, K. Toyoki, D. Billington, H. Okazaki, A. Yasui, W. Ueno, H. Ohashi, S. Hirosawa, Y. Shiratsuchi and T. Nakamura, J. Synchrotron Rad. **25**, 1444 (2018).

[4] D. Billington, K. Toyoki, H. Okazaki, Y. Kotani, T. Fukagawa, T. Nishiuchi, S. Hirosawa and T. Nakamura, Phys. Rev. Mater. **2**, 104413 (2018).

[5] K. Miyazawa, S. Okamoto, T. Yomogita, N. Kikuchi, O. Kitakami, K. Toyoki, D. Billington, Y. Kotani, T. Nakamura, T. Sasaki, T. Ohkubo and Kazuhiro Hono, Acta Materialia **162**, 1-9 (2019).

[6] M. Suzuki, A. Yasui, Y. Kotani, N. Tsuji, T. Nakamura and S. Hirosawa, Acta Materialia **106**, 155-161 (2016).

[7] N. Tsuji, H. Okazaki, W. Ueno, Y. Kotani, D. Billington, A. Yasui, S. Kawaguchi, K. Sugimoto, K. Toyoki, T. Fukagawa, T. Nishiuchi, Y. Gohda, S. Hirosawa, K. Hono and T. Nakamura, Acta Materialia **154**, 25-32 (2018).

Effects of microstructure on magnetization reversal inside hot-deformed permanent magnet

H. Tsukahara[1], K. Iwano[1], C. Mitsumata[2], T. Ishikawa[1], K. Ono[1]
[1]High Energy Accelerator Research Organization (KEK), Tsukuba, Ibaraki 305-0801, Japan
[2]National Institute for Materials Science (NIMS), Tsukuba 305-0047, Japan

Introduction

For the development of high-performance permanent magnet, it is indispensable to know magnetization dynamics inside the permanent magnet. In demagnetization process, magnetization reversals are initialed and domain walls move across inside grains and grain boundaries. Magnetizations are interacted with each other through exchange and dipole fields, and these interactions play important roles in the domain wall displacement. However, the mechanism of magnetization process is not yet fully understood. In this study, we performed large-scale micromagnetic simulation using our simulation code [1] based on Landau–Lifshitz–Gilbert equation and analyzed simulation data to clarify magnetization reversal process inside the hot-deformed magnet.

Model and method

Figure 1(a) shows the simulation model of a nanocrystalline hot-deformed permanent magnet of size 1024 nm × 1024 nm × 512 nm. The simulation model consists of 3,391 tabular grains whose averaged diameter and thickness are 158.4 nm and 32 nm, respectively. Easy axes of the grains are randomly orientated from the z-direction, and the averaged tilt angle of the easy axis is 11.7°. The following $Nd_2Fe_{12}B$ material parameters are assumed in our simulation: saturation magnetization 1281.2 emu/cm^3, uniaxial constant 4.5×10^7 erg/cm^3, exchange stiffness constant 12.5×10^{-7} emu/cm^3, and Gilbert damping constant 1.0. We choose 12.5×10^{-9} emu/cm^3 for inter-grain exchange interaction.

Results

Figure 1(b) shows a snap shot of magnetization reversal process inside the permanent magnet. The magnetization reversals are initiated in some regions where the dipole field of over 1.0T is applied. These dipole fields promote the magnetization reversal. After initiating the magnetization reversal, the domain walls move inside the grains and across the grain boundaries. The domain wall displacement creates pillar-shape magnetization reversal regions owing to the dipole filed. The distribution of the dipole field has relationship with the microstructure of the permanent magnet. Figure 1(c) shows the magnetization reversal and the easy-axis orientations of the grain ($\Delta\theta$) and contacted grain ($\Delta\theta_j^{\max}$). The magnetization is preferentially reversed inside the grains having large $\Delta\theta + \Delta\theta_j^{\max}$.

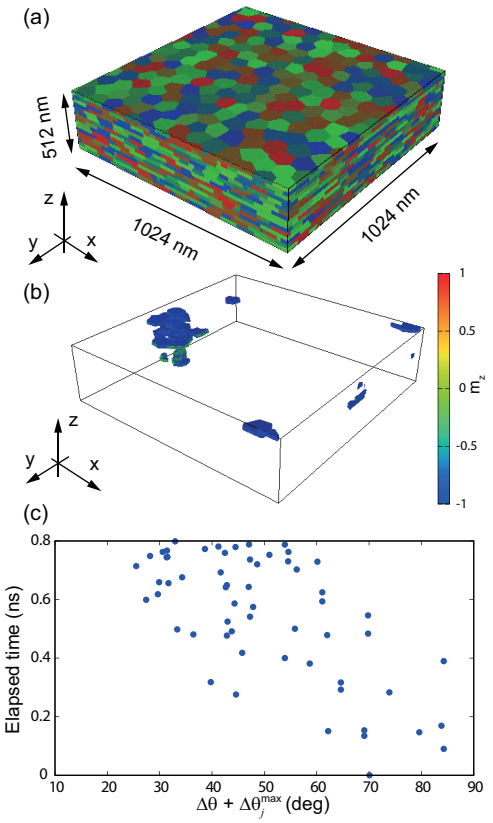

Fig 1: (a) Simulation model of this study, (b) the snap shot of the magnetization reversal process, and (c) the relationship between magnetization reversal and the orientation of the easy-axis of grains.

Acknowledgments

The authors would like to express their sincere thanks to the crew of the Center for Computational Materials Science of the Institute for Materials Research, Tohoku University.

[1] H. Tsukahara, K. Iwano, C. Mitsumata, T. Ishikawa, K. Ono, Phys. Rev. Applied **11**, 014010 (2019).

Defect grain influence on the mechanism of coercivity and its angular dependence of exchange-coupled polycrystalline Nd-Fe-B magnet

J. Li[1], Xin Tang[1], H. Sepehri-Amin[1], T. Ohkubo[1], K. Hono[1]

[1] Elements Strategy Initiative Center for Magnetic Materials, National Institute of Materials Science, Tsukuba 305-0047, Japan

The coercivity mechanism of Nd-Fe-B-based magnet has been in dispute since its discovery. Considering the existence of the defect regions such as the grain boundary (GB), where K_1 is locally damaged or grains are largely misaligned, the nucleation model suggests that the coercivity is determined by the formation of the reversed magnetic domain at these defect regions, whereas the pinning model suggests that domain wall (DW) pinning/depinning process is dominant for the coercivity. In recent years, the finite element micromagnetic simulation method has developed into a strong tool to study the coercivity of Nd-Fe-B magnet with complex microstructure. However, even for a simple case with uniform ferromagnetic GBs, the predicted coercivity by simulation can diverge largely from experimental results, ranging from 1 T to 3.2 T [1-3]. A systematic study is necessary to clarify the physics behind these simulation results.

In this work, we focus on the exchange-coupled Nd-Fe-B magnet, based on the simulations of a three-phase micromagnetic model including the polyhedron Nd-Fe-B grains, the continuous thin ferromagnetic GBs and a defect grain on the model surface (Fig.1 (a)). It is shown that, depending on the anisotropy degradation of the defect grain, K_1^{def}/K_1, both pinning- and nucleation-controlled reversals can appear (Fig.1 (b)). The linear formula, $\mu_0 H_c = \alpha\mu_0 H_c - N_{eff}\mu_0 M_s$, is confirmed to be valid for both pinning- and nucleation-controlled coercivity but with different dominant factor of α. If nucleation starts at a defect grain, α is directly influenced by K_1^{def}/K_1 as indicated by the linear relationship between K_1^{def}/K_1 and coercivity, whereas for pinning-controlled reversal, α is hardly influenced by K_1^{def}/K_1. The simulated angular dependence of coercivity shows strong dependence on the reversal mode (Fig.1 (c)). In a pinning-controlled reversal, the coercivity continuously increases with measurement angle θ, whereas in a nucleation-controlled reversal, the coercivity decreases at small θ but increases again at large θ.

To compare the simulation with experiment, 0.5%-Ga-doped sintered magnets with/without post-sintered annealing [4] are utilized to measure the angular dependence. Our simulation of pinning-controlled model agrees well with the as-sintered sample, indicating the pinning mechanism for the coercivity of this exchange-coupled magnet. In addition, the angular dependence of the post-annealed exchange-decoupled sample will be further discussed, in comparison with our simulation of magnet model with non-ferromagnetic GBs.

References

1) J. Fujisaki, *et al.*, IEEE Trans. Magn. 50 (2014): 1-4.
2) M. Soderžnik, *et al.*, Acta Mater. 135 (2017): 68-76.
3) J. Fischbacher, *et al.*, Scripta Mater. 154 (2018): 253-258.
4) T.T. Sasaki, *et al.*, Scripta Mater. 113 (2016) 218-221.

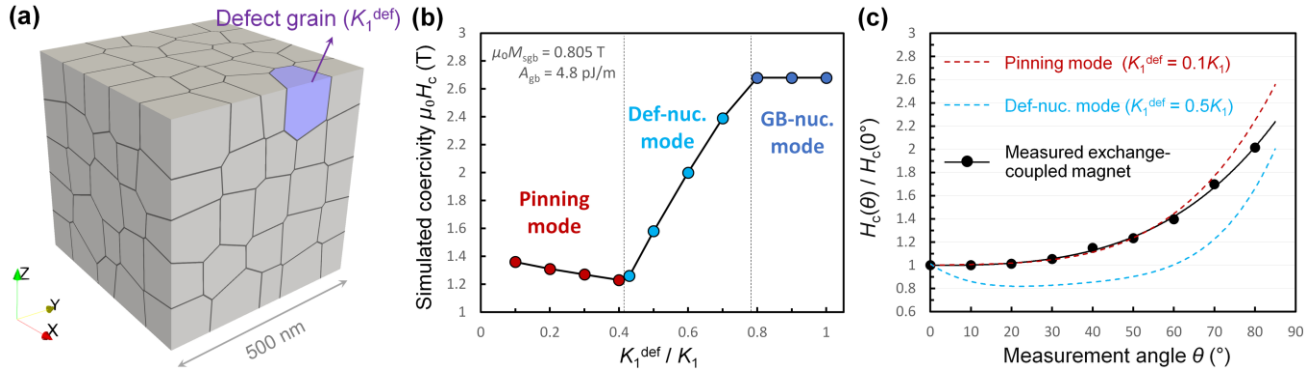

Fig.1 (a) The micromagnetic model of exchange-coupled Nd-Fe-B sintered magnet. (b) Simulated coercivity value as a function of K_1^{def}/K_1. (c) Comparison between simulated and measured angular dependence of coercivity.

Demagnetizing field correction of rare earth permanent magnets using finite element method

J. Fujisaki[1], A. Furuya[1], H. Shitara[1], Y. Uehara[2], K. Kobayashi[3], Y. Hayashi[4], K. Ozaki[5]
[1]Fujitsu Ltd., Kawasaki, 211-8588, Japan
[2]Magnetic Device Laboratory Ltd., Kawasaki, 215-0011, Japan
[3]Shizuoka Institute of Science and Technology, Fukuroi, 437-8555, Japan
[4] Toei Industry Co. Ltd., Machida, 194-0035, Japan
[5]National Institute of Advanced Industrial Science and Technology (AIST), Nagoya, 463-8560, Japan

Among the problems with performance improvement of electric vehicles, recently the accurate measurement of magnetic curves of the rare earth permanent magnets such as Nd-Fe-B sintered magnets[1)] is attracting much attention. The problem is the difficulty of measurement of full loops of permanent magnets having high coercivity using closed magnetic circuit measurements, due to the magnetic saturation of pole piece in apparatus. It is possible to avoid such problem with measurements of open magnetic circuit, such as VSM, and employing the demagnetizing field correction method with single coefficient *N* of the sample (conventional method). Although the above correction method works well for most magnetic materials, there are some cases that the open magnetic circuit curves for Nd-Fe-B sintered magnets are not fully corrected by using conventional method. In order to overcome this problem, many researches on the accurate correction method are being performed[2)]. In this presentation, a new demagnetizing field correction method is proposed and some results are shown.

The detailed algorithm is as follows: First, the mesh model of the magnet and the measured open magnetic circuit hysteresis curve are prepared. Second, temporary closed magnetic circuit curve defined as the following equation is set at all meshes in the model,

$$M_{close}(H) = {M_r}^{open} \tanh\{A(H - {H_c}^{open})\} + B(H - {H_c}^{open}) \quad \cdots\cdots(1)$$

where, ${M_r}^{open}$ and ${H_c}^{open}$ are the remanence and the coercivity of the measured open magnetic circuit curve. *A* and *B* are the parameters that are initially set to zero. Then, the distribution of the demagnetizing field and the magnetization of the mesh model are calculated by using finite element method for all steps of the applied magnetic field. Next, the averaged magnetization of the whole meshes is compared with that of the measured open magnetic circuit curve, and the difference between them is evaluated. Based on the difference, the parameters in Eq. (1) are modified. The procedure explained above is repeated until the difference becomes smaller than the threshold.

The result for 4mm-cubed $Nd_2Fe_{14}B$ sintered magnet is shown in Fig. 1. The dotted curve is the measured closed magnetic circuit curve and the solid one is the calculated closed magnetic circuit curve. Moreover, the long dashed curve is measured by VSM with ceramic superconducting magnet and the dashed one is obtained by convectional method. From Fig. 1, it could be said that the new demagnetizing field correction method is able to reproduce the squareness of the measured closed magnetic circuit curve with higher accuracy than conventional method.

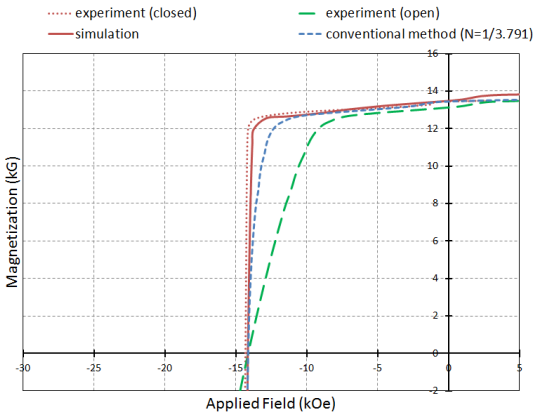

Fig. 1 Demagnetizing field corrected curves and the measured curve

Acknowledgements

This research is supported by Technology Research Association of Magnetic Materials for High-Efficiency Motors (MagHEM), which is consigned by New Energy and Industrial Technology Development Organization (NEDO) of Ministry of Economy, Trade and Industry, Japan.

Reference

1) M. Sagawa, et al, J. Appl. Phys., 55, 2083 (1984)
2) H. Nishio, et al, IEEE Trans. Magn., Vol. 53, No. 4 (2017)

Easy measurement of anisotropy constants for Nd-Fe-B sintered magnet

H. Nishio[1, 2] and K. Machida[1]
[1] Division of Applied Chemistry, Osaka University, Suita 565-0871, Japan
[2] Research Institute for Measurement of Magnetic Materials, Yokohama 240-0026, Japan

1. Introduction To reduce the irreversible demagnetization of Nd–Fe–B sintered magnets at elevated temperatures, it is necessary to significantly improve coercivity (H_{cJ}) which is related to the quadratic (first, K_1) anisotropy constant. Recently easy measurements of anisotropy constants [K_1 and quartic (second, K_2)] have received considerable interest in connection with related fields of applications. We have newly developed useful and simplified torque measurement that efficiently operates in high fields (H) using a superconducting magnet (SCM) in the temperature range of 298-473 K.[1)]

2. Experiment The composition of the sintered magnet used was $Nd_{13.6}Fe_{bal}Co_{1.1}Al_{0.3}B_{5.7}$ with H_{cJ} of 0.99 MA/m and saturation magnetization (J_s) of 1.51 T at 298 K. The composition of the magnet with excellent orientation is considerably close to the $Nd_2Fe_{14}B$ single crystal**,** so that it can be considered as K_1 value makes no great difference. To obtain anisotropy constants, we made use of a new torque magnetometer mounted strain gauges on a rigid pipe (made of Ti) to sense the force (F) in a highly uniform H (0.02%/10 mm cube).[1)] Sample is mounted on the free end of the rigid pipe in the center of SCM. It is only in the case of an ellipsoid that the demagnetizing field becomes uniform for a uniform distribution of magnetization. Thus we chose a sphere (diameter of 7.0 mm) for the shape of sample. To measure the K_1 and K_2 from the results of F obtained from the strain output (ε) using Wheatstone bridge circuit, we ensured angles of inclination (φ) of 45° and 20° to the perpendicular unidirectional H. The torque $L(\varphi)$ obtained from F is equivalent to the values of magnetic torque [$L(\theta)$] curve at θ of 45° and 20°, where θ is the angle between the easy axis and J_s. $L(\theta)$ exerted by the magnetic anisotropy energy of sample can be measured by the mechanical torque [L (= $F \times l_s$)] acting on the rigid pipe, where l_s is the length of the rigid pipe. In highly uniform H, the force (= $M \times \partial H_z/\partial z$) based on magnetic moment (M) does not act on the rigid pipe, because a gradient of H ($\partial H_z/\partial z$) can be disregarded. Therefore, L acting on the rigid pipe is the only $L(\theta)$. $L(\theta)$ of a tetragonal symmetry is generally expressed: $L(\theta) = -(K_1 + K_2)\sin(2\theta) + (K_2/2)\sin(4\theta)$. F was loaded the outside of the SCM by the weight in free end of the rigid pipe mounted horizontally on a vice. The torque proofs were corrected using the product of mass of the weight (10-300 g) and l_s.

3. Results and discussion The large L was almost proportional to ε: $L = 3.839 \times \varepsilon - 0.003$. Fig. 1 shows the strain output for the magnet at φ of 45° and 20°, and the blank sample. The measured values of ε are necessary to make the correction using the values of the blank sample in these respective H (4.8, 5.6, 6.4, and 7.2 MA/m). Fig. 2 shows K_1 of the magnet, which was extrapolated to the infinite H at various temperatures. K_1 and K_2 of the magnet were 4.6 and 0.37 MJ/m^3 at 298 K, respectively. K_1 was in substantially agreement with the published values for the $Nd_2Fe_{14}B$ single crystal.[2)] As the temperature rose to 473 K, these deteriorated remarkably to 1.0 and 0.23 MJ/m^3, respectively. Both K_1 and K_2 decreased as the temperature increased. Anisotropy field of magnet at 298 K was 6.09 MA/m. A significantly higher H than H_A was necessary to obtain H_A for the Nd-Fe-B sintered magnet. Despite the very simple mechanism, this method can measure the large K_1 and K_2 of Nd–Fe–B sintered magnet at elevated temperatures in high H.

Acknowledgment We are grateful to Showa Measuring Instruments Co., Ltd., for helping to mount the strain gauge.

References 1) H. Nishio and K. Machida, IEEE Trans. Magn., **54** (2018) 6000904. 2) D. Givord et al., Solid State Commun., **51** (1984) 857.

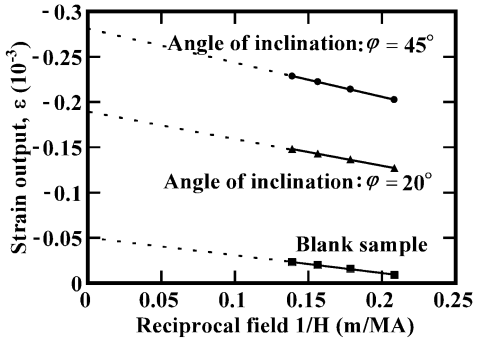

Fig. 1 Plots of strain output versus the reciprocal field at 298 K.

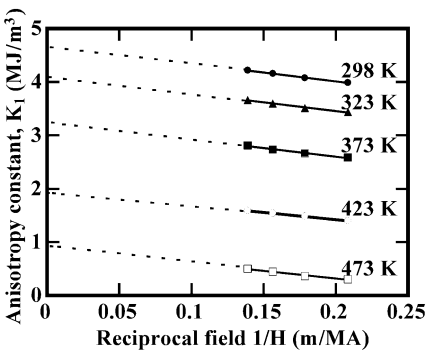

Fig. 2 Plots of the K_1 versus the reciprocal field at 298-473 K.

Potential of RFe_z (z = 9-12) alloys as permanent magnet materials

S. Sakurada
Corporate Research & Development Center, Research & Development Division, Toshiba Corporation

RFe_z compounds (R = rare earth element, z = 9-12) crystalized in the $ThMn_{12}$ structure [1] or the $TbCu_7$ structure [2] have been investigated as promising candidates for next-generation high-performance permanent magnet materials because they can contain large amounts of iron. Some of these compounds are reported to exhibit intrinsic magnetic properties of exceeding that of $Nd_2Fe_{14}B$ [3,4]. We have focused on the crystal phases appearing in such iron-rich R-Fe alloys, their phase stability, and the magnetic properties of these compounds for the last 30 years, and mainly obtained the following results and findings.

(1) The atomic radius of the element occupying the rare-earth site is an important factor to stabilize the $ThMn_{12}$ structure in $RFe_{10}Si_2$ system. The $ThMn_{12}$ phase was found in the system in which the individual rare-earth atomic radius were smaller than those of neodymium in $RFe_{10}Si_2$. In the $(Nd,Zr)Fe_{10}Si_2$ system, zirconium occupies the neodymium site and facilitates the formation of the $ThMn_{12}$ phase owing to the decrease in the atomic radius of the neodymium site [5].

(2) In $(Nd,Zr)Fe_{12-x}Si_x$, the $ThMn_{12}$ phase was not observed at $x \leqq 1$, and the Th_2Ni_{17} phase or the Th_2Zn_{17} phase were observed together with α-Fe. However, in $(R,Zr)(Fe,Co)_{10}$ rapidly quenched alloys (R=Nd, Sm, V_s = 40m/s), almost a single phase with the $TbCu_7$ structure was obtained. The presence of zirconium makes it possible to realize a $TbCu_7$ structure with a high lattice constant ratio c/a of more than 0.87. In the structure, it is believed that a greater number of the dumbbell arrangements of iron atoms exist. $(Sm,Zr)(Fe,Co)_{10}N_x$ prepared by rapid quenching, annealing, and nitogenation exhibited a high saturation magnetization ($\mu_0 M_s$) of 1.70 T and an anisotropy field ($\mu_0 H_a$) of 7.7 T [4].

(3) We have developed isotropic magnet powder with the composition of $(Sm,Zr)(Fe,Co)_zB_{0.1}N_x$ (z = 9-10). A small addition of boron is effective for forming the amorphous phase in the rapidly quenched alloys and for obtaining uniform and fine grains of the $TbCu_7$ phases after annealing. The magnetic properties of these powders are B_r = 1.00-1.07 T, H_{cJ} = 640-880 kA/m, $(BH)_{max}$ = 160-180 kJ/m^3. Isotropic bonded magnets fabricated using such powder show highest $(BH)_{max}$ = 123 kJ/m^3 [6] and are currently commercialized and used in various motors.

(4) Compounds containing a greater number of the dumbbell arrangements of iron atoms such as RFe_{12} having the $ThMn_{12}$ structure and $RFe_{9\text{-}12}$ having the $TbCu_7$ structure tend to be appeared in alloys having the smaller atomic radius of the rare-earth site. However, use of heavy-rare-earth lowers the saturation magnetization. Therefore, it is important to realize a situation similar to the heavy-rare-earth compounds by the substitution of Nd or Sm with the element having a smaller atomic radius such as Zr.

In this presentation, I also mention recent topics on the intrinsic magnetic properties of $RFe_{9\text{-}12}$ compounds and attempts to improve the coercivity, as well as some interesting issues that have not been solved for these compounds.

Reference
1) K. Ohashi et al., IEEE Trans. Magn. 23 (1987) 3101–3103.
2) M. Katter et al., J. Appl. Phys. 70 (1991) 3188-3196.
3) Y. Hirayama et al., Scr. Mater. 138 (2017) 62–65.
4) S. Sakurada et al., J. Appl. Phys. 79 (1996) 4611–4613.
5) S. Sakurada et al., J. Alloys Compd. 187 (1992) 67–71.
6) S. Sakurada et al., Proc. 16th Int. Workshop on RE Magnets and Their Applications (2000) 719-726.

Site preference of dopant elements in rare-earth permanent magnets

Munehisa Matsumoto, Takafumi Hawai, Kanta Ono
Institute of Materials Structure Science, High Energy Accelerator Research Organization, Tsukuba 305-0801

Rare-earth permanent magnets (REPM's) fabricated on the basis of Nd-Fe-B alloys have a problem in temperature resistance of magnetic properties due to the relatively low Curie temperature at 585K of the main-phase compound $Nd_2Fe_{14}B$ and sometimes need expensive elements like Dy in industrial applications for traction motors of electric vehicles to supplement the high-temperature performance. It is desirable to raise the Curie temperature, enhance the temperature resistance of magnetic properties, or/and avoid expensive elements in REPM. While prospective $SmFe_{12}$-based REPM could provide an ideal answer to all of the above wished requests, addition of extra elements seems to be unavoidable to ensure the structural stability of the particular 1:12 crystal structure, among which one of the most typical ones is Ti, yielding $RFe_{11}Ti$ compounds. Here the best compromise in the tradeoff between ferromagnetism and structure stability is pursued. In order to estimate the best possible magnetic performance in the operation temperature range of the REPM compounds, we inspect from first principles the intrinsic magnetic properties and energetics for the site preference of dopant elements in $Nd_2Fe_{14}B$ [1] and in RFe_{12} (R=Sm and Nd) partly aided by experimental data obtained by neutron scattering experiments. We put a focus on the effect of dopant elements on the exchange couplings between rare-earth and Fe-group elements which basically put the most stringent constraint on the utility of the main-phase ferromagnet [2]. Contrasting trends between Ti and Co in the preferred sites are elucidated referring to the magnetic exchange couplings between dopant and host atoms. Implications of those numerically and experimentally observed trends on the robustness of localized magnetic moments on Fe all through the sample fabrication processes are discussed. The best compromise with $Sm(Fe,Co)_{11}Ti$ and $Nd(Fe,Co)_{11}TiN_x$ is inspected.

References

1) MM, preprint [arXiv:1812.10945].
2) MM, H. Akai, Y. Harashima, S. Doi, and T. Miyake, J. Appl. Phys. **119**, 213901 (2016).

Magnetic anisotropy constants and magnetic moments of Fe in $ThMn_{12}$-type $Sm(Fe_{1-x}Co_x)_{12}$ compounds

D. Ogawa[1], T. Yoshioka[2], S. Li[3], T. Ueno[3], S. Sakai[3], T. Mitsui[3],
Y. K. Takahashi[1], H. Tsuchiura[2], S. Hirosawa[1] and K. Hono[1]
1 Elements Strategy Initiative Center for Magnetic Materials (ESICMM), National Institute for Materials Science, Tsukuba, 300-0047 Japan
2 Department of Applied Physics, Tohoku University, Sendai, 980-8579, Japan
3 National Institutes for Quantum and Radiological Science and Technology QST, Hyogo, 679-5148/Takasaki 370-1292, Japan

The $ThMn_{12}$-type the $Sm(Fe_{1-x}Co_x)_{12}$ ($0 \leqq x \leqq 0.2$) compound films exhibit intrinsic hard magnetic properties superior to those of $Nd_2Fe_{14}B$ for x=0.2[1]. Therefore, it is important to investigate the origin of intrinsic magnetic properties such as magnetic anisotropy and magnetization of the $Sm(Fe_{1-x}Co_x)_{12}$ compound and their temperature dependence. In this work, we evaluated the magnetic anisotropy constant of the $Sm(Fe_{1-x}Co_x)_{12}$ films by using the anomalous Hall effect (AHE) torque measurements. The results were compared with the ab-initio calculations of the crystal field parameters at the Sm site using a spin model of $Sm(Fe_{1-x}Co_x)_{12}$ compounds. We also evaluated the magnetic moment of each Fe site in $Sm(Fe_{1-x}Co_x)_{12}$ films and their temperature dependence using the total reflection synchrotron-radiation Mössbauer spectroscopy method.

Epitaxial $Sm(Fe_{1-x}Co_x)_{12}$ films were prepared by an ultra-high vacuum magnetron co-sputtering system with the stacking structure of MgO(001) substrate/V(001)(10nm)/$Sm(Fe_{1-x}Co_x)_{12}$(288-325nm)/V(2nm) (x=0, 0.07, 0.2). Anomalous Hall effect was measured by using a physical property magnetic system (PPMS) with a maximum magnetic field of 14T. ^{57}Fe Mössbauer spectra were measured at RT and 250°C on the beamline BL11XU at SPring-8.

Fig.1 shows the temperature dependence of K_1 and K_2 for the $Sm(Fe_{1-x}Co_x)_{12}$ films with various Co contents. While K_1 monotonically decreases with increasing temperature, K_2 changes its sign from negative to positive with increasing temperature. This behavior is consistent with the effective spin model approach[2] based on the ab-initio calculation. Fig.2 shows the internal magnetic field of each Fe site and their magnetic moment as a function of Co content at RT and 250°C from the analysis of Mössbauer data. The fitting was performed using three independent spectra for the 8i, 8j and 8f Fe-sites. The site dependence of internal magnetic fields follows the sequence 8i > 8j > 8f, which corresponds to the previous Mössbauer measurement in $ThMn_{12}$ structure[3]. When the moment of Sm is assumed to be zero, the estimated saturation magnetization value without Co (x=0) is about 1.65T at RT, which is in a good agreement with the previously reported value[1]. The enhancement of magnetic moments was observed at each Fe site as increasing the Co content, which could be the reason for the magnetization enhancement of $Sm(Fe_{1-x}Co_x)_{12}$ compound.

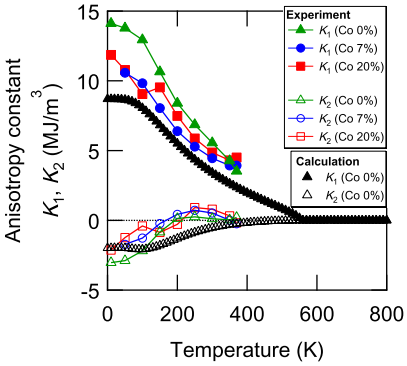

Fig.1 K_1, K_2 for $Sm(Fe_{1-x}Co_x)_{12}$ films as a function of temperature

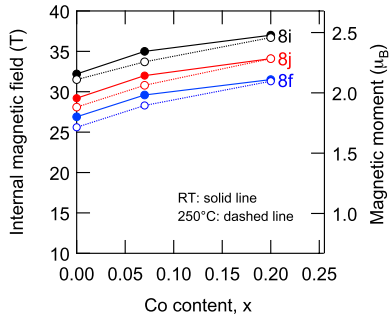

Fig.2 Internal magnetic field and magnetic moment at each Fe site for $Sm(Fe_{1-x}Co_x)_{12}$ films

Reference
1) Y. Hirayama, Y.K. Takahashi, S. Hirosawa and K. Hono, Scr. Mater., 138, 62 (2017).
2) T. Yoshioka and H. Tsuchiura, Appl. Phys. Lett. 112, 162405 (2018)
3) M. Gjoka, V. Psycharis, E. Devlin, D. Niarchos, G. Hadjipanayis, J. Alloys Compd. 687, 240-245 (2016).

Origin of the magnetisation enhancement by Zr addition in $(Sm_{1-x}Zr_x)(Fe_{0.8}Co_{0.2})_{12}$ studied using X-ray magnetic circular dichroism

A. Martin-Cid[1,2], S. Kobayashi[1,2], K. Toyoki[1,2], D. Ogawa[2], Y.K. Takahashi[2], S. Hirosawa[2], K. Hono[2], T. Nakamura[1,2]

[1]Japan Synchrotron Radiation Research Institute, 1-1-1 Kouto, Sayo, 679-5198, Japan

[2]Elements Strategy Initiative Center for Magnetic Materials (ESICMM), National Institute for Materials Science, Tsukuba 305-0047, Japan

The scarcity of rare earth elements (RE) categorized as critical raw materials have stimulated the search for new rare earth-free/lean alloys alternatives for Nd-Fe-B based permanent magnets. Some of $REFe_{12}$ compounds with tetragonal $ThMn_{12}$ (1:12) structure show high magnetocrystalline anisotropy [2] and an inherent lean content of rare earths (7.7 at.%) compared with $Nd_2Fe_{14}B$ (11.8 at.%) can induce high magnetisation. However, binary $REFe_{12}$ is not thermodynamically stable and a ternary element in substitution of Fe is needed to obtain the 1:12 structure in bulk, which reduces the saturation magnetisation of the compound [3]. Recently, it has been reported that substitution of Sm with Zr stabilises the 1:12 structure without decreasing magnetisation in the certain range of Zr concentration [4,5].

In this work, we have measured XMCD spectra at the Fe and Co $L_{2,3}$-edges and the Sm $M_{4,5}$-edges in (001) oriented epitaxial $(Sm_{1-x}Zr_x)(Fe_{0.8}Co_{0.2})_{12}$ (x = 0, 0.14 and 0.26) films grown on a (001)-oriented V underlayer deposited on a MgO(001) single crystalline substrate, as reported by Hirayama et al. [6]. The magnetisations of these films at room temperature (RT) are summarized in Table 1. The XMCD experiment was performed at BL25SU of SPring-8. The element specific magnetisation was calculated by the sum rule analysis for the XMCD spectra recorded at RT and 20 K, which showed an increase of the magnetisation for the sample with x = 0.14. The present results show that the small addition of Zr of 0.14 enhances the magnetic moment of Fe atoms by a 6% while a large change of a 23% of the magnetic moment of Sm is found. The relatively low concentration of Sm in the 1:12 structure compared with Fe makes that the total magnetisation of the alloy is driven mainly by the enhancement of the magnetic moments of Fe, with a total increase of a 6.3%. Since the intensity of the resonant absorption (not shown here), which is proportional to the number of the 3*d* electron, doesn't change significantly, the charge transfer between Fe and Zr can be discarded as a dominant factor for this enhancement. This observation likely suggests that Zr substitution mainly affects the crystal structure such as the increase of local Fe-Fe distances or the weakening of Fe 3*d* – Sm 5*d* hybridisation, which leads to the enhancement of the ferromagnetic coupling.

Table 1.- Summary of the magnetisation measured at RT by SQUID and the magnetisation and magnetic moments of each element calculated by XMCD which was recorded at RT.

Zr content	Magnetisation (T) SQUID	Magnetisation (T) XMCD	Magnetic moment m (μ_B)		Δm (%)
x = 0	1.78	1.75	Fe	2.32	-
			Co	1.53	-
			Sm	-0.42	-
x = 0.14	1.87	1.86	Fe	2.46	6.0
			Co	1.55	1.3
			Sm	-0.32	23.8

Reference

1) A.M. Gabay, et al., Scr. Mater. **154** (2018) 284-288.
2) R. Verhoef, et al., J. Magn. Magn. Mater. **75** (1988) 319–322.
3) S. Suzuki, et al., J. Magn. Magn. Mater. **401** (2016) 259–268.
4) T. Kuno, et al., AIP Adv. **6** (2016), 025221.
5) Y. Hirayama, et al., Scripta Materialia **138** (2017) 62–65.

Grain size reduction of $SmFe_{12}$-based powders; toward development of bulk high-performance permanent magnet

H. Sepehri-Amin, I. Dirba, T. Ohkubo, and K. Hono
Elements Strategy Initiative Center for Magnetic Materials, NIMS, Tsukuba 305-0047, Japan

Recent investigations on intrinsic magnetic properties of $SmFe_{12}$-based compounds with the $ThMn_{12}$ structure have shown that $Sm(Fe_{0.8}Co_{0.2})_{11}Ti$ and $Sm_{0.8}Zr_{0.2}(Fe_{0.8}Co_{0.2})_{11.5}Ti_{0.5}$ alloy compounds have comparable intrinsic hard magnetic properties and better temperature dependence with those of $Nd_2Fe_{14}B$ [1]. The remaining challenge is to further develop those intrinsic properties into practically useful extrinsic ones, particularly coercivity. In this work, we focused on reduction of the grain size of $SmFe_{12}$-based compounds by jet-milling and investigated the phase stability of the powders with different particle size [2,3]. We also introduce a few grain boundary phases that can exchange decouple $SmFe_{12}$-based grains in order to obtain high coercivity.

Starting alloys with compositions of $Sm(Fe_{0.8}Co_{0.2})_{11}Ti$, $Sm(Fe_{0.8}Co_{0.2})_{10.5}Ga_{0.5}Ti$, and $Sm(Fe_{0.8}Co_{0.2})_{10.5}Cu_{0.5}Ti$ were prepared by induction melting. The ingots were crushed into coarse powders and hydrogen decrepitated to reduce the particle size below 100 μm. The powders were jet-milled for the particle refinement study. The magnetic properties were measured using a SQUID-VSM. Microstructure of the samples were analyzed using SEM/FIB (Carl Zeiss 1540EsB) and TEM (Titan G2 80-200).

We used three different compositions of $SmFe_{12}$-based alloys and demonstrated fine, anisotropic, single-crystalline $SmFe_{11}Ti$-based micro-particles with high roundness by jet-milling using N_2 gas. The smallest particle size of 2.7±0.6 μm and roundness of 0.73±0.13 was achieved in the case of $Sm(Fe_{0.8}Co_{0.2})_{10.5}Cu_{0.5}Ti$, as shown in Fig. 1 (a). Although the $ThMn_{12}$-type structure is preserved even at high milling gas pressures, the coercivity of the powders remained below 0.2 T. The intergranular phase that originally exist in the as-cast alloy is removed or changed to an amorphous surface phase as shown in Fig. 1 (b). Detailed characterization of jet-milled powders using BF and HAADF-STEM showed that the $SmFe_{12}$-based jet-milled powders experience plastic deformation through crystallographic slip and the formation of slip bands during jet-milling process (Fig. 1(c)). Observed projection of the atoms in HAADF-STEM image (Fig. 1(c)) show that Sm atoms are missing in the slip bands indicating the crystal structure is damaged at the slip bands. These defects decrease local magnetocrystalline anisotropy compared to the matrix region that can be nucleation centers for the formation of reverse magnetic domains and thus limiting the coercivity. We will show that possible solutions for minimizing defect formation are, using lower milling gas pressure, performing a post-annealing step or using Ga doped starting alloy. Temperature-dependent XRD results showed that unlike large sized powders (>100μm), jet-milled powders with a size of smaller than 5μm decompose from the surface at temperatures above 600ºC resulting in formation of α-Fe. We will also show low-melting alloys with good wettability with $SmFe_{12}$-powders that can be used for metal bonded magnets.

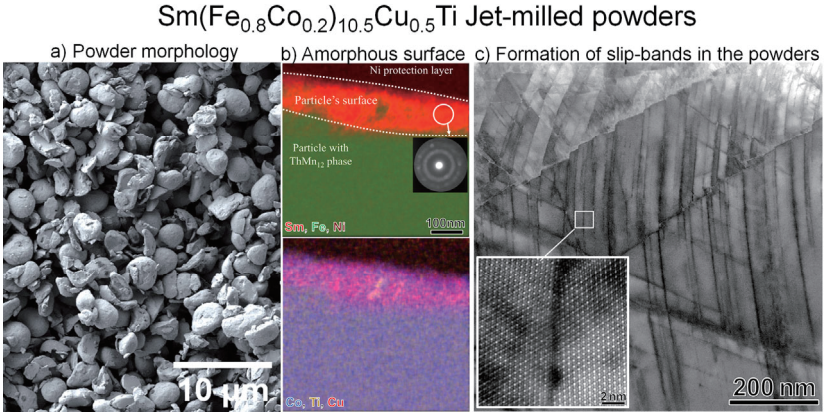

Figure 1: (a) Secondary electron (SE) SEM image showing morphology of jet-milled powders, (b) STEM-EDS maps and micro-diffraction pattern showing amorphous Sm-Cu rich phase at the surface of jet-milled powders, and (c) bright field (BF)-STEM and high resolution HAADF-STEM image (inset) obtained from inside of the jet-milled powders with composition of $Sm(Fe_{0.8}Co_{0.2})_{10.5}Cu_{0.5}Ti$.

Reference
[1] P. Tozman, H. Sepehri-Amin *et al.* Acta Mater. 153 (2018) 534.
[2] I. Dirba, H. Sepehri-Amin *et al.* Acta Mater. 165 (2019) 9. [3] I. Dirba, H. Sepehri-Amin *et al.* Submitted.

Development of Sm-Fe-N bulk magnets showing high maximum energy products

Ryo Matsunami, Masashi Matsuura, Nobuki Tezuka, Satoshi Sugimoto
(Tohoku University)

Introduction

$Sm_2Fe_{17}N_3$ compound shows high J_s, high H_A and high T_C, therefore the $Sm_2Fe_{17}N_3$ based bulk magnet is expected to show high thermal stability with high $(BH)_{max}$. However, it is well known that preparation of bulk $Sm_2Fe_{17}N_3$ based magnets cannot be obtained by conventional sintering process because of decomposition of this compound above around 600 °C. For obtaining bulk Sm-Fe-N magnets, applying metal binder having low melting temperature and/or applying Spark-Plasma-Sintering (SPS) have been reported by many researchers. Recently, our group and AIST group have reported that decreasing oxygen content in $Sm_2Fe_{17}N_x$ based magnets is effective for suppressing deterioration of coercivity after heat treatment [1-4]. In our previous study, we applied Arc plasma deposition (APD) and SPS for preparing Zn-bonded Sm-Fe-N bulk magnets, and we reported $(BH)_{max}$ of 153 kJm^{-3} with H_{cJ} of 1.1 MAm^{-1} for Zn-bonded Sm-Fe-N magnet and $(BH)_{max}$ of 179 kJm^{-3} with H_{cJ} of 0.8 MAm^{-1} for binder-less Sm-Fe-N magnet [4]. We also reported that the Hydrogen-Plasma-Metal-Reaction (HPMR) method is useful for preparation of fine Zn particles with low oxygen content [2]. Thus, in this study, we applied HPMR method and SPS process for preparing Zn-bonded Sm-Fe-N magnets, and we obtained high $(BH)_{max}$ Sm-Fe-N bulk magnets.

Experimental Procedure

Sm_2Fe_{17} coarse powder was pulverized by ball milling. The fine Sm-Fe powder was nitrided under N_2 gas at 450 °C. Zn fine powder was prepared by the HPMR method. After mixing Sm-Fe-N and Zn powder, the Sm-Fe-N/Zn mixed powder was pressed under magnetic field, and it was sintered by SPS with conditions of 750 MPa at 380-440 °C.

Results and Discussion

Oxygen content of the Sm-Fe-N powder was 0.22 wt%, and remanence and coercivity of the powder was 151 Am^2kg^{-1} and 0.72 MAm^{-1}, respectively. Magnetic properties of the Zn-free Sm-Fe-N magnet were H_{cJ} of 0.86 MAm^{-1} and $(BH)_{max}$ of 188 kJm^{-3}, respectively. It is shown that coercivity of the magnet did not decrease after sintering because of low oxygen content. The 10 wt%-Zn Sm-Fe-N/Zn bonded magnets showed excellent magnetic properties of $(BH)_{max}$ = 200 kJm^{-3} with H_{cJ} = 1.28 MAm^{-1}. Compared with previous studies, this $(BH)_{max}$ is highest level of Sm-Fe-N bulk magnets showing high H_{cJ}, simultaneously. The $(BH)_{max}$ of the Zn-bonded magnet was higher than that of Zn-free magnet in this study because of higher relative density. Therefore, Zn binder is effective for not only increasing coercivity but also increasing density of the magnets. Temperature coefficient of coercivity of the magnets were evaluated, and -0.38 %/K and -0.35 %/K for Zn-free and Zn-bonded magnets were obtained, respectively. Consequently, it is successfully obtained high performance Sm-Fe-N bulk magnets.

Acknowledgement

This study was partially supported by the Future Pioneering Program “Development of magnetic material technology for high-efficiency motors” (MagHEM) commissioned by the NEDO, and the Elements Strategy Initiative Center for Magnetic Materials (ESICMM) under the outsourcing project of MEXT.

Reference

1) R. Soda *et al.*, *AIP Adv.*, **6** (2016) 115108.
2) M. Matsuura, *et al., J. Magn. Magn. Mater*, **452** (2018) 243.
3) Y. Nishijima *et al.*, Collected abstract of the 40th Annual Conference on Magnetics in Japan, 2016, p.254.
4) M. Matsuura, *et al., J. Magn Mang. Mater,* **467** (2018) 64.